

1  
2  
3 IMPROVED SIMULATION OF  
4 PRECIPITATION IN THE TROPICS  
5 USING A MODIFIED BMJ SCHEME IN  
6 WRF MODEL

7  
8  
9  
10  
11 RICARDO FONSECA

12 Earth Observatory of Singapore, Nanyang Technological University

13 TENGFEI ZHANG

14 School of Physical and Mathematical Sciences, Nanyang Technological University

15 KOH TIEH YONG†

16 Earth Observatory of Singapore, Nanyang Technological University

17 School of Physical and Mathematical Sciences, Nanyang Technological University

18  
19  
20  
21  
22†Corresponding author address: Koh Tieh Yong, Earth Observatory of Singapore, Nanyang Technological University,  
N2-01a-15, 50 Nanyang Avenue, Singapore 639798. E-mail: [kohty@ntu.edu.sg](mailto:kohty@ntu.edu.sg).

## ABSTRACT

23  
24  
25  
26  
27  
28  
29  
30  
31  
32  
33  
34  
35  
36  
37  
38  
39  
40  
41

The successful modelling of the observed precipitation, a very important variable for a wide range of climate applications, continues to be one of the major challenges that climate scientists face today. When the Weather Research and Forecasting (WRF) model is used to dynamically downscale the Climate Forecast System Reanalysis (CFSR) over the Indo-Pacific region, with analysis (grid-point) nudging, it is found that the cumulus scheme used, Betts-Miller-Janjić (BMJ), produces excessive rainfall suggesting that it has to be modified for this region. Experimentation has shown that the cumulus precipitation is not very sensitive to changes in the cloud efficiency but varies greatly in response to modifications of the temperature and humidity reference profiles. A new version of the scheme, denoted “modified BMJ” scheme, where the humidity reference profile is more moist, was developed. In tropical belt simulations it was found to give a better estimate of the observed precipitation as given by the Tropical Rainfall Measuring Mission (TRMM) 3B42 dataset than the default BMJ scheme for the whole tropics and both monsoon seasons. In fact, in some regions the model even outperforms CFSR. The advantage of modifying the BMJ scheme to produce better rainfall estimates lies in the final dynamical consistency of the rainfall with other dynamical and thermodynamical variables of the atmosphere.

## 42 1. INTRODUCTION

43

44 One of the major challenges facing regional climate modelers today is the accurate  
45 representation of the observed rainfall, in particular in areas with complex topography and  
46 land-sea contrasts such as the Maritime Continent (hereafter MC). The MC, which consists of  
47 the Malay Peninsula, the Greater and Lesser Sunda Islands and New Guinea, comprises small  
48 landmasses with elevated terrain and shallow seas. This is a region of conditional instability  
49 that plays an important role in the large-scale atmospheric circulation (Ramage, 1968). When  
50 used to simulate the climate of these regions, given their coarse horizontal resolutions, Global  
51 Climate Models (hereafter GCMs) fail to capture many of the factors and processes that drive  
52 regional and local climate variability, including the regional topography, and so Regional  
53 Climate Models (hereafter RCMs), forced by GCMs or re-analysis data, are used instead, to  
54 better study the climate of the MC.

55

56 When running a RCM forced with coarse resolution data as lateral boundary conditions,  
57 and without any further constraints, the fields in the interior can be quite different from the  
58 driving fields (Bowden et al., 2012) meaning that some form of relaxation in the interior,  
59 either analysis (Stauffer and Seaman, 1990, 1991) or spectral (Waldron et al., 1996; von  
60 Storch et al., 2000) nudging, is required to keep the RCM from diverging too far from the  
61 coarse-grid data. In WRF, and in both analysis and spectral nudging, the horizontal winds ( $u$ ,  
62  $v$ ) and the potential temperature perturbation ( $\theta'$ ) are relaxed towards a reference state.  
63 However, while in the former water vapour mixing ratio ( $q_v$ ) is also nudged, in the latter the  
64 geopotential height perturbation ( $\phi$ ) is relaxed instead. The reason why moisture is not  
65 nudged in spectral nudging is because of its spatial distribution: it can have pronounced  
66 horizontal and especially vertical variations that are likely to be missed out by the coarse

67 resolution re-analyses used to force the RCMs (Miguez-Macho et al., 2005). Given the  
68 importance of the water vapour distribution for the simulation of the tropical climate, analysis  
69 nudging is employed with the four fields nudged every 6h on a time-scale of ~1h, a typical  
70 time-scale used in nudging experiments (Stauffer and Seaman, 1991) and comparable to the  
71 critical time-scale needed to properly reproduce the large-scale flow in the tropics (Hoskins et  
72 al., 2012). Nudging is only applied above the level of 800hPa, and excluding the Planetary  
73 Boundary Layer (hereafter PBL), as this configuration is found to give the best results for this  
74 region (Jeff Lo, pers. comm.). In addition, experimentation has shown that the precipitation  
75 over Southeast Asia is not very sensitive to the choice of the radiation, PBL, microphysics  
76 and land surface schemes but varies greatly with the choice of the cumulus scheme, with the  
77 Betts-Miller-Janjić (hereafter BMJ) scheme giving the smallest biases compared to the Kain-  
78 Fritsch (Kain and Fritsch, 1990, 1993; Kain, 2004) and Grell-Devenyi (Grell and Devenyi,  
79 2002) schemes (Jeff Lo, pers. comm.). However, even when interior nudging is employed,  
80 WRF overestimates the observed rainfall, as given by TRMM 3B42 version 6 (Huffman et  
81 al., 2007), as seen in *Figure 1*. Here the rainfall rate over Southeast Asia averaged over the  
82 2008 boreal summer (June-September, JJAS) for TRMM and the WRF experiments with and  
83 without analysis nudging is shown. As can be seen, without interior nudging the model  
84 produces excessive precipitation in particular in the monsoon regions of southern Asia and to  
85 the east of the Philippines as a result of an incorrect representation of the large-scale  
86 atmospheric circulation (not shown). When analysis nudging is employed the phase of the  
87 WRF precipitation is similar to that of TRMM's but the model continues to overestimate its  
88 amplitude. Given that most of the rainfall in these runs is generated by the cumulus scheme,  
89 the excessive precipitation produced suggests that the cumulus scheme may have to be  
90 modified at least for this region and possibly for the global tropics. The modification of the  
91 BMJ scheme to yield better tropical rainfall estimates will be addressed in this paper which

92 will also necessitate a comprehensive discussion of the BMJ scheme as implemented in  
93 WRF.

94  
95 Despite recent improvements, much work is still needed to successfully develop an accurate  
96 representation of cumulus convection in numerical models. There are essentially two widely  
97 used types of convection parameterization schemes in weather and climate models: mass-flux  
98 or moisture convergence schemes (e.g. Arakawa and Schubert, 1974; Kain and Fritsch, 1990,  
99 1993, Kain, 2004; Emanuel, 2001) and adjustment schemes (e.g. Betts, 1986, Betts and  
100 Miller, 1986, Janjić, 1994). In the former a one-dimensional cloud model is used to compute  
101 the updraft and downdraft mass fluxes and processes such as entrainment and detrainment are  
102 also normally considered. In contrast to these increasingly complex parameterizations which  
103 can involve detailed models of cloud processes, convective adjustment schemes take an  
104 “external” view of convection and simply relax the large-scale environment towards  
105 reference thermodynamic profiles. One of such schemes is the Betts-Miller (hereafter BM)  
106 scheme that was originally developed by Alan Betts and Martin Miller in the 1980’s and later  
107 modified by Zaviša Janjić in the 1990’s to yield the current BMJ scheme. Janjić introduced a  
108 parameter called “cloud efficiency” that acts to reduce the precipitation in order to provide a  
109 smoother transition to grid-resolved processes.

110  
111 The WRF model (Skamarock et al., 2008), a fully compressible and non-hydrostatic  
112 model, is used in this work. WRF uses a terrain-following vertical coordinate derived from  
113 the hydrostatic pressure and surface pressure and the Arakawa-C grid staggering for  
114 horizontal discretization. It is a community model used in a wide variety of applications  
115 including idealized simulations (e.g. Steele et al., 2013), hurricane research (e.g. Davis et al.,  
116 2008), regional climate research (e.g. Chotamonsak et al., 2011, 2012), weather forecasts  
117 (e.g. Done et al., 2004) and coupled atmosphere-ocean modelling (e.g. Samala et al., 2013).

118 Here it is used to investigate the sensitivity of the cumulus precipitation to modifications  
119 made to the BMJ scheme and to assess the performance of the “modified BMJ” scheme in  
120 tropical belt simulations.

121  
122 In Section 2 details about the model setup and methods used are presented. A discussion  
123 of the BMJ scheme is given in section 3 while the results obtained in sensitivity experiments  
124 are shown in Section 4. In section 5 the focus is on the modified scheme’s performance in  
125 tropical belt experiments and in section 6 the main conclusions are presented.

## 126 2. MODEL, DATASETS AND DIAGNOSTICS

127  
128

129 In this study WRF is initialized with CFSR 6-hourly data (Saha et al., 2010; this data was  
130 downloaded from the Research Data Archive at the National Center for Atmospheric  
131 Research, Computational and Information Systems Laboratory, available online at  
132 <http://rda.ucar.edu/datasets/ds093.0/>), horizontal resolution of  $0.5^\circ \times 0.5^\circ$ , and is run for 1 day  
133 (2<sup>nd</sup> March – 3<sup>rd</sup> March 2008), 1 month (1<sup>st</sup> April – 30<sup>th</sup> April 2008), 6 months (1<sup>st</sup> April 2008  
134 – 30<sup>th</sup> September 2008) and 10 months (1<sup>st</sup> June 2008 – 31<sup>st</sup> March 2009) with a 1-day spin-  
135 up in the first set of experiments and a 1-month spin-up time in the last three prior to the  
136 stated simulated periods. The year of 2008 is chosen as according to Ummenhofer et al.  
137 (2009) it is a neutral year with respect to both El Niño-Southern Oscillation (ENSO) and  
138 Indian Ocean Dipole (IOD). By choosing a neutral year, the impact of climatic anomalies is  
139 minimized. The physics parameterizations used include the WRF double-moment five-class  
140 microphysics scheme (Lim and Hong, 2010), the Rapid Radiative Transfer Model for Global  
141 (RRTMG) models for both shortwave and longwave radiation (Iacono et al., 2008), the  
142 Yonsei University planetary boundary layer (Hong et al., 2006) with Monin-Obukhov surface  
143 layer parameterization (Monin and Obukhov, 1954), the four-layer Noah land surface model  
144 (Chen and Dudhia, 2001) and to parameterize cumulus convection the BMJ scheme (Janjić,  
145 1994). In all model runs 6-hourly sea surface temperature (hereafter SST) and monthly values  
146 of vegetation fraction and surface albedo are used. WRF is also run with a simple prognostic  
147 scheme of the sea surface skin temperature (Zeng and Beljaars, 2005) which takes into  
148 account the effects of the sensible, latent and radiative fluxes as well as diffusion and  
149 turbulent mixing processes in the vertical. In all model simulations nudging is applied at the  
150 lateral boundaries over a nine-gridpoint transition zone while in the top 5 km Rayleigh

151 damping is applied to the wind components and potential temperature on a time-scale of 5 s  
152 (Skamarok et al., 2008).

153 The spatial domain on Mercator projection used for the 1-day, 1-month and 4-month  
154 diagnostics, shown in *Figure 1*, extends from central Africa to the East Pacific and from  
155 about 25°S to 25°N with a horizontal grid spacing of 24km, while for the 10-month  
156 experiments a tropical belt extending from about 42°S to 45°N with a horizontal resolution of  
157 30km is used. In all model runs 37 vertical levels, more closely spaced in the PBL and in the  
158 tropopause region, are used with the model top at 30hPa and the highest un-damped layer at  
159 about 70hPa. The time-step used is 1 min and the output is archived every 1h. Analysis  
160 nudging is applied to the horizontal winds ( $u$ ,  $v$ ), potential temperature perturbation ( $\theta'$ ) and  
161 water vapour mixing ratio ( $q_v$ ). These fields are relaxed towards CFSR above 800hPa  
162 excluding the PBL on a time-scale of 1h. The WRF rainfall is evaluated against the 3-hourly  
163 instantaneous multi-satellite rainfall estimates from TRMM, at a horizontal resolution of  
164  $0.25^\circ \times 0.25^\circ$ , while all other fields are compared with CFSR. The model outputs on pressure  
165 and surface levels are bilinearly interpolated to the CFSR and TRMM grids for evaluation.

166 The model's performance is assessed with different verification diagnostics including the  
167 model bias, normalized bias ( $\mu$ ), correlation ( $\rho$ ), variance similarity ( $\eta$ ) and normalized error  
168 variance ( $\alpha_\epsilon$ ). The bias is defined as the discrepancy between the model and observations  
169 while the normalized bias is given by the bias divided by the standard deviation of the  
170 discrepancy between the model and observations (when  $|\mu| < 0.3$  the contribution of the bias  
171 to the total error is less than ~5% and the biases will not be significant). The correlation is a  
172 measure of the phase agreement between the model and observations. The variance similarity  
173 is an indication of how the signal amplitude given by the model agrees with that observed and  
174 is defined as the ratio of the geometric mean to the arithmetic mean of the modelled and

175 observed variances. The normalized error variance is the variance of the error arising from  
176 the disagreements in phase and amplitude, normalized by the combined modelled and  
177 observed signal variances. The best model performance corresponds to zero bias and  $\alpha_\epsilon$  and  
178 to  $\rho$  and  $\eta$  equal to 1. These diagnostics are defined in equations (A1) – (A5) in *Appendix A*.

### 179 3. BETTS–MILLER–JANJIĆ (BMJ) CUMULUS SCHEME

180  
181

182 The BMJ scheme is an adjustment scheme where the essential principle lies in the  
183 relaxation of the temperature and humidity profiles towards reference thermodynamic  
184 profiles and precipitation is obtained as a necessary consequence from the conservation of  
185 water substance. The equations and factors used in the BMJ scheme, as we found  
186 implemented in WRF version 3.3.1, are given in the *Appendix B* which the reader is  
187 encouraged to consult. We found two main existing differences in WRF's default  
188 implementation from the original formulation as defined in Betts (1986) and Janjić (1994):

189

190 • In the definition of the potential temperature reference profile, (B8), the factor  $\alpha$  used is 0.9  
191 as opposed to 0.85 as suggested by Betts (1986). A larger  $\alpha$  leads to a warmer and more  
192 moist reference profile and therefore to a reduction in the precipitation produced by the  
193 cumulus scheme;

194

195 • The factor  $F_S$ , used in the definition of the humidity reference profile for deep convection,  
196 (B12) – (B14), is set to 0.85 while in Janjić (1994), a value of 0.6 is used. The smaller  $F_S$  is,  
197 the more moist the humidity reference profile will be and, therefore, the smaller the amount  
198 of precipitation generated by the scheme.

199

200 In section 4.1 the sensitivity of the precipitation produced by this scheme to  $\alpha$  and  $F_S$ , as well  
201 as to the cloud efficiency  $E$  and the convective adjustment time-scale  $\tau$ , will be investigated.

202

## 203 4. SENSITIVITY EXPERIMENTS

204

### 205 4.1 ONE-DAY DIAGNOSTICS

206

207 The aim of these experiments is to investigate the sensitivity of the precipitation  
208 produced by the BMJ scheme to changes in some of the parameters used in the scheme. In  
209 particular, as the default WRF-BMJ implementation scheme produces excessive rainfall over  
210 Southeast Asia, as shown in *Figure 1*, in this section different ways of reducing the cumulus  
211 precipitation are explored in order to determine which ones are more efficient.

212 WRF is run from 00UTC on 1<sup>st</sup> March to 00UTC on 3<sup>rd</sup> March 2008 with the first day  
213 regarded as model spin-up. The results are shown in *Figure 2*. Here the precipitation rate  
214 obtained with the default BMJ scheme as implemented in WRF version 3.3.1 (control run) is  
215 plotted together with the modification in the rainfall rate for ten experiments with a modified  
216 BMJ scheme: in the first experiment the sensitivity to the convective adjustment time-scale  $\tau$   
217 is explored, in the next three the sensitivity to modifications in some of the parameters used  
218 in  $F(E)$  (namely  $c_l$ ,  $E_l$  and  $F_l$ ) is assessed while in the other six experiments the sensitivity  
219 to changes in the temperature and humidity reference profiles through modifications in  $\alpha$ ,  $F_S$   
220 and  $F_R$  is examined.

221 Given that the precipitation produced by the BMJ scheme is proportional to  $F(E)$ , (B7), a  
222 linear function of the cloud efficiency,  $E$ , and inversely proportional to the adjustment time-  
223 scale  $\tau$ , the cumulus rainfall can be reduced by decreasing  $F(E)$  and increasing  $\tau$ . The former  
224 can be achieved by lowering the constant  $c_l$  used in the definition of the cloud efficiency  
225 (B5), reducing  $F_l$  or increasing  $E_l$  (a higher  $E_l$  also means a more moist humidity reference  
226 profile and less rainfall). In *Figure 2* the difference in the rainfall rate, with respect to the

227 default WRF-BMJ implementation, when  $\tau$  is doubled ( $\tau=80\text{min}$ ),  $c_1$  is set to one tenth of its  
228 original value ( $c_1=0.5$ ) as well as when  $E_1 = 0$  and  $F_1 = 0.4$  is shown. The impact of changing  
229 these parameters on the cumulus rainfall is negligible. Similar results are obtained to changes  
230 in  $F_2$  and  $E_2$  (not shown) which is not surprising as changing  $F_2$  and  $E_2$  is equivalent to  
231 changing  $\tau$  and  $c_1$ , respectively. Hence, the precipitation produced by the BMJ scheme is not  
232 very sensitive to changes in  $F(E)$  and  $\tau$ .

233 The rainfall produced by the BMJ scheme can also be modified by changing the reference  
234 temperature and/or humidity profiles. The temperature reference profile, defined in (B8),  
235 includes a parameter  $\alpha$  that when increased will give a warmer (and hence more moist)  
236 profile and therefore a reduction in the precipitation. The precipitation can also be decreased  
237 by making the humidity reference profile more moist which can be achieved by reducing  $F_S$   
238 or  $F_R$ , (B12) – (B14). The default value of  $F_R$  is 1 and an experiment is performed where it is  
239 reduced to 0.9. As shown in *Figure 2(e)*, the BMJ scheme's rainfall is not sensitive to  
240 changes in  $F_R$ . The default values of  $F_S$  and  $\alpha$  are 0.85 and 0.9, respectively, and experiments  
241 are performed where  $F_S$  is reduced to 0.6, the value suggested by Janjić (1994), and 0.3, and  
242  $\alpha$  is increased to 1.2 and 1.5. One last run in which both parameters are modified ( $F_S$  is  
243 reduced to 0.6 and  $\alpha$  increased to 1.5) is also performed. As seen in *Figure 2*, the BMJ  
244 scheme's rainfall is very sensitive to changes in these two parameters, in particular to  $\alpha$ : in  
245 fact, when  $\alpha$  is set to 1.5 the cumulus scheme produces almost no precipitation (i.e., the  
246 convection shuts down).

247 In conclusion, in 1-day runs it is found that the precipitation produced by the BMJ  
248 scheme is not sensitive to changes in the cloud efficiency  $E$  and  $F(E)$  but varies greatly when  
249 the humidity and temperature reference profiles are modified. In the next section results from  
250 2-month runs performed with a modified BMJ scheme using the new values of  $F_S$  and  $\alpha$  to

251 further assess how the rainfall produced in those runs compares to that obtained with the  
252 default WRF-BMJ implementation and observations (TRMM).

## 253 4.2 ONE-MONTH DIAGNOSTICS

254

255 The impact on precipitation due to changes in the temperature and humidity reference  
256 profiles will now be assessed in 1-month runs. WRF is run from 1<sup>st</sup> March to 30<sup>th</sup> April 2008,  
257 with the first month being regarded as spin-up. The precipitation rate averaged over April for  
258 the experiments with the default BMJ scheme and five modified BMJ schemes is shown in  
259 *Figure 3*. In the first two the humidity reference profile is more moist than in the default  
260 version of the scheme, with  $F_S$  changed to 0.6 and 0.3, but no changes are made to the  
261 temperature reference profile; in the following two the temperature reference profile is  
262 warmer (and hence the humidity reference profile is more moist) with  $\alpha$  set to 1.2 and 1.5;  
263 finally, in the last experiment  $F_S$  is reduced to 0.6 and  $\alpha$  increased to 1.5.

264 When the default WRF-BMJ implementation is used the model overestimates the observed  
265 rainfall mainly in the MC, eastern Indian Ocean, central tropical Pacific and in the South  
266 Pacific Convergence Zone (hereafter SPCZ). However, the other diagnostics are quite high  
267 with typical values of 0.7–0.8 for  $\rho$ , 0.8–0.9 for  $\eta$  and 0.2–0.3 for  $\alpha_\epsilon$  and suggesting that  
268 WRF captures well the phase and variance of the observed rainfall resulting in small errors in  
269 the rainfall pentad series. As expected, in regions that typically receive very little  
270 precipitation, such as the Australian desert and south-eastern parts of the Arabian Peninsula,  
271 these diagnostics are rather low scores.

272 Regarding the experiments with a modified BMJ scheme, when  $F_S$  is set to 0.6, the value  
273 recommended by Janjić (1994), there is a much better agreement with TRMM except over  
274 the high terrain (in particular in the islands of New Guinea and Borneo) where the model  
275 overestimates the observed rainfall. In these regions the precipitation is mostly produced by  
276 the microphysics scheme (not shown). However, there is not much of an improvement in the

277 other three diagnostics as they are already good. When a smaller value of  $F_S$  is used,  
278 corresponding to an even more moist humidity reference profile, there is a significant  
279 reduction in the precipitation over the whole domain, with the model now producing less  
280 rainfall than TRMM, with a slight worsening of the other diagnostics in particular of  $\eta$  and  $\alpha_\epsilon$   
281 and over the eastern Indian Ocean, MC and West Pacific. As found in the previous section,  
282 the sensitivity of the cumulus precipitation to changes in the temperature reference profile is  
283 even larger: when  $\alpha$  is increased to 1.2 the scheme produces very little rainfall and a further  
284 increase to 1.5 leads to precipitation being confined mainly to the ITCZ, SPCZ and the high  
285 terrain, indicating that the convection nearly shuts down. For these experiments there is a  
286 significant deterioration of the other three diagnostics in particular of  $\eta$  and  $\alpha_\epsilon$ . When  $\alpha$  is  
287 increased to 1.5 and  $F_S$  decreased to 0.6 the model performance is similar to that obtained  
288 when only  $\alpha$  is set to 1.5 but drier than when only  $F_S$  is set to 0.6 stressing the fact that  $\alpha$  is  
289 the limiting factor and not  $F_S$ .

290 In conclusion, in two-month experiments it is found that, out of the different options  
291 considered, the best agreement with TRMM is obtained when  $F_S$  is set to 0.6, the value  
292 recommended by Janjić (1994), corresponding to a more moist humidity reference profile  
293 while keeping  $\alpha$  at its default value of 0.9. This new implementation of the BMJ scheme,  
294 hereafter called “modified” BMJ, will now be tested in 6-month runs.

295

296

297

### 298 4.3 FOUR-MONTH DIAGNOSTICS

299

300 In 1-month runs it is found that the best agreement in the rainfall rate between WRF and  
301 TRMM is obtained when  $F_S$  is set to 0.6, corresponding to a more moist humidity reference  
302 profile. In this section the performance of this modified BMJ scheme will be tested in 6-  
303 months runs initialised on 1<sup>st</sup> April with a focus on the boreal summer season, June to  
304 September. In addition, this experiment is also repeated with no interior nudging and relaxing  
305 the water vapour mixing ratio, horizontal winds and potential temperature perturbation  
306 separately towards CFSR. The results are shown in *Figure 4*.

307 As seen in *Figure 4*, when the modified BMJ scheme is used there is a significant  
308 improvement in the representation of the observed rainfall, as given by TRMM, compared to  
309 that obtained with the default WRF-BMJ implementation: the positive biases with the default  
310 BMJ scheme over the MC and Southeast Asia are corrected when the modified BMJ scheme  
311 is used. In fact, with the modified BMJ scheme the model bias is only significant mainly over  
312 the high terrain, where most of the rainfall is actually produced by the microphysics scheme.  
313 There is an exception around Sri Lanka, however, where there is little precipitation in TRMM  
314 but WRF produces a considerable amount of rainfall and therefore the biases will be  
315 significant here. There is also some improvement in the other verification diagnostics (not  
316 shown).

317 In all WRF experiments discussed so far analysis nudging was employed. However, it is of  
318 interest to assess the modified BMJ scheme's performance when no interior nudging is used.  
319 The fourth and fifth rows of *Figure 4* show the precipitation obtained with the default and  
320 modified BMJ schemes but with no interior nudging applied and they convey a very different  
321 picture: in this case there is almost no improvement in the simulation of the observed

322 precipitation when the modified BMJ scheme is used as the decrease in the cumulus rainfall  
323 is offset by an increase in the microphysics precipitation. This is an important result that  
324 suggests any change made to the BMJ scheme will be fruitless without interior (analysis)  
325 nudging. In the default configuration, as stated in section 2, the horizontal winds ( $u,v$ ),  
326 potential temperature perturbation ( $\theta'$ ) and water vapour mixing ratio ( $q_v$ ) are relaxed towards  
327 CFSR. Three additional experiments are performed with the modified BMJ scheme where  
328 these variables are nudged separately. As shown in *Figure 4*, the crucial variable that has to  
329 be relaxed is the water vapour mixing ratio,  $q_v$ : in fact, when only this field is nudged the  
330 precipitation produced by the model is very similar to that obtained when all four fields are  
331 relaxed toward CFSR with similar contributions to rainfall from the cumulus and  
332 microphysics schemes. If analysis nudging is only applied to the temperature or horizontal  
333 winds there are much larger biases. When only the former is nudged there is excessive  
334 precipitation from microphysics off the east coast of India and the Bay of Bengal, as in the  
335 experiment with no interior nudging, because of an incorrect representation of the large-scale  
336 circulation, as well as to the north-east of New Guinea with the ITCZ in the Pacific displaced  
337 southwards. When only the horizontal winds are nudged there is excessive precipitation in a  
338 region aligned in the southwest-northeast direction to the west of Sumatra as well as along  
339 the ITCZ in the Pacific as a result of excessive moisture in those regions (not shown). In  
340 these two experiments, and as opposed to the ones where only  $q_v$  or all four fields are relaxed,  
341 the microphysics rainfall gives a contribution as large as, or even larger than, the cumulus  
342 rainfall to the total precipitation. It can be concluded that it is crucial to properly represent the  
343 water vapour mixing ratio in the tropics in order to simulate the observed precipitation. It is  
344 also important to stress that here the focus has just been on the precipitation and when only  
345 one of the referred fields is nudged separately there are noticeable errors in others and hence

346 all four fields have to be nudged in order for the model to correctly simulate the atmospheric  
347 circulation over Southeast Asia (Bowden et al., 2013).

## 348 5. TROPICAL BELT EXPERIMENTS

349

350 The performance of the modified BMJ will now be assessed for the whole tropics and  
351 for 11-months initialised on 1<sup>st</sup> May 2008 with the first month as spin-up. We focus on the  
352 boreal summer monsoon season, JJAS 2008, and winter monsoon season, December to  
353 February (hereafter DJFM) straddling 2008 and 2009. The results are shown in *Figure 5*.

354 In the boreal summer, the precipitation produced by WRF in Southeast Asia in the tropical  
355 belt experiments is similar to that obtained in the smaller domain runs performed at 24km  
356 horizontal resolution shown in *Figure 4*. With the default WRF-BMJ implementation, WRF  
357 produces excessive precipitation over most of Southeast Asia and the East Equatorial Pacific  
358 with rainfall biases that are also significant over high terrain, in particular over the East  
359 African Highlands, the Himalayas, the Arakan Mountains in western Myanmar and the  
360 Andes. When the modified BMJ scheme is employed, there is a significant improvement with  
361 the biases being now restricted to the high terrain as well as around Sri Lanka (as explained  
362 before in section 4). The change in the other verification diagnostics ( $\rho$ ,  $\eta$  and  $\alpha_\epsilon$ ) is small as  
363 they are already relatively good.

364 As also shown in *Figure 5*, similar results are obtained for the boreal winter season: with the  
365 default WRF-BMJ implementation the model overestimates the precipitation in the MC and  
366 along the SPCZ, but these biases are largely corrected when the modified BMJ scheme is  
367 used. However, over land areas such as the Amazon and south-central Africa, and despite  
368 some improvement, the model continues to overestimate the observed precipitation. This is  
369 because the convective clouds produced by the BMJ scheme are radiatively transparent so  
370 that surface temperature remains too warm during rainfall, an issue that will be addressed in a  
371 subsequent paper. As was the case for the summer season, very little improvement is seen in

372  $\rho$ ,  $\eta$  and  $\alpha_\epsilon$  when the modified BMJ scheme is used with typical correlations of 0.6–0.8,  
373 variance similarity close to 1 and normalized error variances of 0.3–0.4 over most of the  
374 domain except in regions with light and irregular amounts of precipitation, such as eastern  
375 side of sub-tropical Pacific and Atlantic Oceans and deserts in northern and southern Africa  
376 and Arabian Peninsula, Tibetan plateau, Australia and South America. The southern Amazon  
377 basin experiences dry season in boreal summer and so  $\eta$  and  $\alpha_\epsilon$  indicate bad model  
378 performance in that season

379 The improvement in the representation of the observed precipitation when the modified BMJ  
380 scheme is used is not just confined to Southeast Asia in the boreal summer season, but takes  
381 place across the whole tropics and in both monsoon seasons. It is important to note that not  
382 all biases are corrected, in particular over high terrain where most rainfall is produced by the  
383 microphysics scheme. In these regions WRF is known to overestimate the rainfall, as  
384 discussed in Teo et al. (2011), and an accurate simulation of the precipitation requires higher  
385 horizontal resolution to properly resolve the orography which we cannot afford  
386 computationally in this larger domain.

## 387 6. CONCLUSIONS

388

389 The accurate modelling of precipitation, in particular over complex topography and  
390 regions with strong land-sea contrasts such as the MC, continues to be one of the major  
391 challenges that atmospheric scientists face today. In this study the BMJ scheme, a convective  
392 adjustment scheme where temperature and humidity are relaxed towards reference profiles, as  
393 implemented in WRF version 3.3.1, is modified so that the precipitation produced by the  
394 model is in better agreement with that observed as given by TRMM.

395 In 1-day runs the sensitivity of the precipitation to changes in some of the parameters  
396 used in the cumulus scheme is investigated. It is found that the rainfall is not sensitive to:  $\tau$ ,  
397 the convective time-scale;  $F(E)$ , a linear function of the cloud efficiency;  $F_R$ , the upper limit  
398 to dehumidification by rain formation. The same is not the case when the temperature and  
399 humidity reference profiles are modified by changes in the parameters  $\alpha$  and  $F_S$ . When the  
400 temperature reference profile is warmer (corresponding to a larger  $\alpha$ ) and/or the humidity  
401 reference profile is more moist (corresponding to a larger  $\alpha$  or a smaller  $F_S$ ) there is a  
402 decrease in the convective rainfall and vice-versa.

403 In 1-month experiments it is found that, out of the different values of  $\alpha$  and  $F_S$  considered, the  
404 best agreement of the model's precipitation with the one given by TRMM is obtained with a  
405 more moist humidity reference profile with the parameter  $F_S$  set to 0.6, the value suggested  
406 by Janjić (1994). This new value is adopted as the modification to the BMJ scheme in  
407 subsequent work.

408 From the 4-month diagnostics during JJAS 2008, the rainfall generated by WRF with the  
409 modified BMJ scheme is found to be in close agreement with that of TRMM. In fact, the  
410 biases are now restricted to high terrain where most of the rainfall is generated by the

411 microphysics scheme. In these experiments analysis nudging is applied in the interior of the  
412 domain. Experimentation showed that with no interior nudging the decrease in the rainfall  
413 given by the cumulus scheme is mostly offset by an increase in the microphysics rainfall.  
414 This result shows that any changes made to the BMJ scheme will only have an impact in the  
415 precipitation if some form of nudging in the interior of the model domain is applied. It is also  
416 found that the rainfall obtained when only specific humidity is nudged is similar to that  
417 obtained when wind and perturbation potential temperature are additionally nudged stressing  
418 the importance of modelling well the water vapour distribution in the tropics to successfully  
419 produce the observed rainfall.

420 The performance of the modified BMJ scheme is further assessed in tropical belt  
421 experiments with the model run from 1<sup>st</sup> May 2008 to 31<sup>th</sup> March 2009 with a focus on the  
422 boreal summer monsoon, JJAS, and boreal winter monsoon, DJFM. It is found that for both  
423 seasons and for the whole tropics, with the modified BMJ scheme the model gives a better  
424 estimate of the observed precipitation than the default WRF-BMJ implementation. However,  
425 WRF continues to overestimate the observed rainfall over high terrain where a higher  
426 horizontal resolution is needed to properly resolve the orography. Although there is a  
427 significant reduction in the bias with the modified BMJ scheme, the other three verification  
428 diagnostics considered ( $\rho$ ,  $\eta$  and  $\alpha_\epsilon$ ) do not show much of an improvement as they are  
429 already good.

430 To conclude, the modified BMJ scheme gives a better representation of the observed  
431 rainfall for the whole tropics in both winter and summer seasons, and will be of a great value  
432 to the research community working on tropical dynamics. Progress has also been made in  
433 understanding how the BMJ scheme, as implemented in WRF, interacts with other physics  
434 schemes, in particular with the microphysics scheme.

435 **APPENDIX A: VERIFICATION DIAGNOSTICS**

436

437 
$$BIAS = \langle \mathbf{D} \rangle = \langle \mathbf{F} \rangle - \langle \mathbf{O} \rangle \quad (A1)$$

438

439 
$$\mu = \frac{\langle \mathbf{D} \rangle}{\sigma_D} \quad (A2)$$

440

441 
$$\rho = \frac{1}{\sigma_O \sigma_F} \langle (\mathbf{F} - \langle \mathbf{F} \rangle) \cdot (\mathbf{O} - \langle \mathbf{O} \rangle) \rangle, \quad -1 \leq \rho \leq 1 \quad (A3)$$

442

443 
$$\eta = \frac{\sigma_O \sigma_F}{\frac{1}{2}(\sigma_O^2 + \sigma_F^2)}, \quad 0 \leq \eta \leq 1 \quad (A4)$$

444

445 
$$\alpha_\epsilon = 1 - \rho\eta = \frac{\sigma_D^2}{\sigma_O^2 + \sigma_F^2}, \quad 0 \leq \alpha \leq 2 \quad (A5)$$

446

447 In the equations above  $\mathbf{D}$  is the discrepancy between the model forecast  $\mathbf{F}$  and the  
 448 observations  $\mathbf{O}$ ;  $\sigma_X$  is the standard deviation of  $X$ ;  $\mu$  is the normalized bias;  $\rho$  is the  
 449 correlation coefficient;  $\eta$  is the variance similarity;  $\alpha_\epsilon$  is the normalized error variance.

450 More information about these diagnostics can be found in Koh et al. (2012).

451

452

453 **APPENDIX B: BMJ EQUATIONS FOR DEEP CONVECTION IN WRF**

454 The equations shown in this section are the ones used in the BMJ scheme in WRF Version  
 455 3.3.1 and are based on Betts (1986) and Janjić (1994).

456 In this cumulus scheme as explained in Betts (1986), the model first assesses whether there is  
 457 Convective Available Potential Energy (CAPE) present and whether the cloud is sufficiently  
 458 thick (i.e.,  $L_B - L_T > 2$  or  $p_B - p_T > 10hPa$  where  $L_B$  and  $L_T$  are the cloud-base and cloud-  
 459 top model levels and  $p_B$  and  $p_T$  the correspondent pressure levels;  $L_B$  is defined as the model  
 460 level just above the Lifting Condensation Level (LCL) and has to be at least 25hPa above the  
 461 surface whereas  $L_T$  is defined as the level at which CAPE is maximum (i.e., level of neutral  
 462 buoyancy, LNB) for the air parcel with the maximum equivalent potential temperature  $\theta_E$  in  
 463 the depth interval  $[PSFC, PSFC \times 0.6]$  where  $PSFC$  is the surface pressure. If that is not the  
 464 case there will be no convection and the scheme will abort. If all those conditions are met, the  
 465 cloud depth is compared to a minimum depth given by

$$D_{min} = 200hPa \left( \frac{PSFC}{1013hPa} \right) \quad (B1)$$

466  
 467 If the cloud depth is smaller than  $D_{min}$ , shallow convection is triggered; otherwise, deep  
 468 convection is considered. In both shallow and deep convection (Betts, 1986), temperature and  
 469 humidity fields are adjusted as follows

$$\begin{aligned} \Delta T_{BM} &= T_{REF} - T \\ \Delta q_{BM} &= q_{REF} - q \end{aligned} \quad (B2)$$

470  
 471 where  $\Delta T_{BM}$  and  $\Delta q_{BM}$  are the Betts' adjustment of temperature  $T$  and specific humidity  $q$  in a  
 472 model layer. Thus, the problem is reduced to defining the reference temperature and specific

473 humidity reference profiles  $T_{ref}$  and  $q_{ref}$  for shallow and deep convection. In the BMJ  
 474 scheme rainfall is only produced by deep convection which is the topic of this appendix.

475

## 476 RAINFALL

477 The BM scheme conserves enthalpy meaning that

$$\sum_{p_T}^{p_B} (c_P \Delta T_{BM} + L_{WV} \Delta q_{BM}) \Delta p_L = 0 \quad (B3)$$

478 where  $c_P$  is the specific heat at constant pressure for dry air assumed to be constant;  $L_{WV}$  is  
 479 the latent heat of vaporisation for water vapour;  $\Delta p_L$  is the thickness of the model layer  
 480 bounded by the model level indices  $L$  and  $L + 1$  in pressure coordinate. The total mass of  
 481 water substance is conserved and hence in the original BM scheme (Betts, 1986) the rainfall  
 482 is given by

$$\Delta P_{BM} = \frac{1}{g \rho_w} \sum \Delta q_{BM} \Delta p_L \quad (B4)$$

484

485

486 where  $\rho_w$  is the density of liquid water;  $g$  is the acceleration of free fall.

487 In Janjić (1994), a parameter called cloud efficiency,  $E$ , is introduced and is defined as

$$E = c_1 \frac{\bar{T} \Delta S}{c_P \sum \Delta T_{BM} \Delta p_L} \quad (B5)$$

488

489 with

$$\bar{T} = \frac{\sum T_m \Delta p_L}{p_{bottom} - p_{top}}$$

$$\Delta S = \sum \left( \frac{c_P \Delta T_{BM} + L_{WV} \Delta q_{BM}}{T_m} \right) \Delta p_L$$

$$T_m = T + \frac{\Delta T_{BM}}{2}$$

490

491 where  $\bar{T}$  is the weighted mean temperature of the cloudy air column;  $\Delta S$  is the entropy change  
 492 per unit area for the cloudy air column multiplied by  $g$ ;  $T_m$  is the mean temperature over the  
 493 time-step;  $c_1$  is a non-dimensional constant estimated experimentally and set to 5. All  
 494 summation symbols refer to summing over all cloudy layers [ $L_B, L_T$ ].

495 The denominator of (B5) is proportional to the single time-step rainfall from a model layer in  
 496 the original BM scheme, (B4), and hence the cloud efficiency reduces when there is a  
 497 propensity for heavy rain, partly correcting the tendency to over-predict intense rainfall in the  
 498 original BM scheme.

499

500 In the default WRF-BMJ implementation, the precipitation,  $\Delta P$ , and the adjustments in  
 501 temperature and humidity,  $\Delta T$  and  $\Delta q$ , over one cumulus time-step  $\Delta t$  are given by

$$\begin{cases} \Delta P = \Delta P_{BM} F(E) \Delta t / \tau \\ \Delta T = \Delta T_{BM} F(E) \Delta t / \tau \\ \Delta q = \Delta q_{BM} F(E) \Delta t / \tau \end{cases} \quad (B6)$$

502

503 where  $F(E)$  is a linear function of the cloud efficiency given by

$$F(E) = \left( 1 - \frac{\Delta S_{min}}{\Delta S} \right) \left[ F_1 + (F_2 - F_1) \left( \frac{E' - E_1}{E_2 - E_1} \right) \right] \quad (B7)$$

504

505 with  $E'$  constrained to be in the range  $[E_1, E_2]$ :

$$E' = \begin{cases} E_1 & \text{if } E \leq E_1 \\ E & \text{if } E_1 \leq E \leq E_2 \\ E_2 & \text{if } E \geq E_2 \end{cases}$$

506

507 The constant  $F_1 = 0.7$  is determined experimentally and  $F_2 = 1$  for the chosen value of  
 508  $\tau$  while  $E_1 = 0.2$  is determined empirically in Janjić (1994) and  $E_2 = 1$  for the chosen value  
 509 of  $c_1$ . It is important to note that in Janjić (1994),  $F(E)$  does not depend on the entropy  
 510 change unlike the implementation we found in WRF version 3.3.1. In (B6)  $\tau$  is the convective  
 511 adjustment time-scale set to 40 min (Betts, 1986).

512 If the change in entropy is small (or even negative), i.e.  $\Delta S < \Delta S_{min} = 10^{-4} JK^{-1}m^{-1}s^{-2}$ ,  
 513 or very little (perhaps even negative) rainfall is obtained, i.e.  $\sum \Delta T \Delta p_L \leq$   
 514  $10^{-7} Kkgm^{-1}s^{-2}$ , shallow convection is triggered; otherwise, the BMJ scheme proceeds  
 515 with deep convection. The reader is referred to Janjić (1994) for the documentation on  
 516 shallow convection which we are not concerned with in this work.

517

## 518 **REFERENCE PROFILES FOR DEEP CONVECTION**

519 The first-guess potential temperature reference profile  $\theta_{REF}^f$  for deep convection used in the  
 520 BMJ scheme is assumed to have a vertical gradient that is a fixed fraction  $\alpha$  of the vertical  
 521 gradient of saturated equivalent potential temperature  $\theta_{ES}$  following a moist virtual adiabat  
 522 (i.e. isopleth of virtual equivalent potential temperature) from the cloud base up to the  
 523 freezing level. Above the freezing level,  $\theta_{REF}^f$  slowly approaches and reaches the  
 524 environmental  $\theta_{ES}$  at the cloud top. Thus,  $\theta_{REF}$  given is prescribed by

$$\theta_{REF}^f(p_B) = \theta(p_0, T_0)$$

525

$$\left\{ \begin{array}{l} p_M \leq p_L < p_B: \quad \theta_{REF}^f(p_L) = \theta_{REF}^f(p_{L-1}) + \alpha [\theta_{ES}(p_L) - \theta_{ES}(p_{L-1})] \\ p_T \leq p_L < p_M: \quad \theta_{REF}^f(p_L) = \theta_{ES}(p_L) - \frac{p_L - p_T}{p_M - p_T} \{ \theta_{ES}(p_M) - \theta_{REF}^f(p_M) \} \end{array} \right. \quad (B8)$$

526  
527 where  $p_M$  denotes the pressure at the freezing model level,  $p_L$  denotes the pressure at any  
528 model level in the cloudy air column (such that  $L$  increases upwards from  $p_B$  to  $p_T$ ) and  
529  $p_0$  and  $T_0$  the pressure and temperature at the level from which the air parcel is lifted. In the  
530 first equation the constant  $\alpha$ , according to Betts (1986), is equal to 0.85 but in the default  
531 WRF implementation it is set to 0.9, corresponding to a steeper  $d\theta_{REF}/dp$  or a statically  
532 more stable profile. This choice of 0.9 for  $\alpha$  was made when the scheme was tuned to the  
533 model over the North American region (Zaviša, pers. comm.).

534 The corresponding first-guess reference temperature profile is

$$T_{REF}^f(p_L) = \theta_{REF}^f(p_L) \Pi(p_L) \quad (B9)$$

535  
536 with

$$\Pi(p_L) = \left( \frac{10^5 \text{Pa}}{p_L} \right)^{-R/c_p}$$

537  
538 where  $\Pi(p_L)$  is the Exner's function (divided by  $c_p$ ) for pressure  $p_L$  and  $R$  is the specific gas  
539 constant for dry air.

540 At pressure  $p_L$  equal or lower than 200hPa, the humidity field is not adjusted by the BMJ  
541 scheme. At pressure  $p_L$  larger than 200hPa in the convecting column, the first-guess reference  
542 specific humidity,  $q_{REF}^f(p_L)$ , is prescribed by the lifting condensation level,  $p_L + \wp(p_L)$ , of  
543 an air parcel with  $\theta_{REF}(p_L)$  and  $q_{REF}^f(p_L)$  at pressure  $p_L$ ,

$$\begin{cases} q_{REF}(p_L) = q(p_L) & \text{if } p_L \leq p_{200} \\ q_{REF}^f(p_L) = q^*(\theta_{REF}^f(p_L), p_L + \wp(p_L)) & \text{if } p_L > p_{200} \end{cases} \quad (B10)$$

544

545 where  $p_{200}$  is the pressure of a model level just smaller or equal to 200hPa. With the help of  
 546 Tetens' formula (Tetens, 1930), the saturated specific humidity  $q^*$  is given by

$$q^*(\theta_{REF}^f(p_L), p_L + \wp(p_L)) = \left( \frac{379.90516 \text{ Pa}}{p_L + \wp(p_L)} \right) EXP \left\{ 17.2693882 \left( \frac{\theta_{REF}^f(p_L) - \frac{273.16 \text{ K}}{\Pi(p_L + \wp(p_L))}}{\theta_{REF}^f(p_L) - \frac{35.86 \text{ K}}{\Pi(p_L + \wp(p_L))}} \right) \right\} \quad (B11)$$

547

548 The more negative  $\wp(p_L)$  is, the drier the reference profile is at pressure level  $p_L$ .  $\wp(p_L)$  is  
 549 piecewise linearly interpolated between the values at the cloud bottom,  $\wp_B$ , freezing level,  
 550  $\wp_M$ , and cloud top,  $\wp_T$ , which are in turn parameterized as linear functions of cloud  
 551 efficiency  $E$  as follows:

$$\wp_B = (-3875 \text{ Pa}) \left[ F_S + (F_R - F_S) \left( \frac{E' - E_1}{E_2 - E_1} \right) \right] \quad (B12)$$

$$\wp_M = (-5875 \text{ Pa}) \left[ F_S + (F_R - F_S) \left( \frac{E' - E_1}{E_2 - E_1} \right) \right] \quad (B13)$$

$$\wp_T = (-1875 \text{ Pa}) \left[ F_S + (F_R - F_S) \left( \frac{E' - E_1}{E_2 - E_1} \right) \right] \quad (B14)$$

552

553 The constants in Pa above were determined by Janjić (1994) and are not varied in this work.  
 554

555 In the WRF version 3.3.1 implementation, the parameter  $F_R$  is set to 1 while  $F_S$  is set to 0.85,  
 556 an empirically determined value over continental USA (Zaviša, pers. comm.), while in the  
 557 Janjić (1994)  $F_S = 0.6$ . Evidently, with a higher value of  $F_S$ , the formulation yields more  
 558 negative  $\wp(p_L)$  and a drier reference humidity profile for each cloud efficiency,  $E < E_2$ .

559

560

561 **ACKNOWLEDGMENTS**

562 We are thankful to Bob Dattore (UCAR) for his help in downloading CFSR data through the  
563 CISL RDA website. This work comprises Earth Observatory of Singapore contribution no.  
564 85. It is supported by the National Research Foundation Singapore and the Singapore  
565 Ministry of Education under the Research Centres of Excellence initiative. Special thanks are  
566 owed to Chee Kiat Teo, Yudha Djamil, Shunya Koseki, Jagabandhu Panda, Fang Wan, Ken  
567 Tay and Xianxiang Li who generously made many constructive suggestions.

568

569

570 **REFERENCES**

571

572 Arakawa, A. and Schubert, W. H.: Interaction of a cumulus cloud ensemble with the large-scale  
573 environment, Part I. *J. Atmos. Sci.*, 31, 674-701, 1974

574

575 Betts, A. K.: A new convective adjustment scheme. Part I: Observational and theoretical basis. Non-  
576 precipitating cumulus convection and its parameterization, *Q. J. R. Meteorol. Soc.*, 112, 677-691,  
577 1986.

578

579 Betts, A. K. and Miller, M. J.: A new convective adjustment scheme. Part II: Single column tests using  
580 GATE wave, BOMEX, ATEX and arctic air-mass data sets, *Q. J. R. Meteorol. Soc.*, 112, 693-709,  
581 1986.

582

583 Bowden, J. H., Otte, T. L., Nolte, C. G. and Otte, M. J.: Examining Interior Analysis nudging  
584 Techniques Using Two-Way Nesting in the WRF Model for Regional Climate Modeling, *J. Climate*  
585 25, 2805-2823, 2012.

586

587 Bowden, J. H., Nolte, C. G. and Otte, T. L.: Simulating the impact of the large-scale circulation on the  
588 2-m temperature and precipitation climatology, *Clim. Dyn.* 40, 1903-1920, 2013.

589

590 Chen, F. and Dudhia, J.: Coupling an advanced land surface–hydrology model with the Penn State–  
591 NCAR MM5 modeling system. Part I: Model implementation and sensitivity, *Mon. Wea. Rev.*, 129,  
592 569-585, 2001.

593

594 Chotamonsak, C., Salathe E. P., Kreasuwan, K. and Chantara, S.: Evaluation of Precipitation  
595 Simulations over Thailand using a WRF Regional Climate Model, *Chiang Mai J. Sci.*, 39, 623-638,  
596 2012.

597

598 Chotamonsak, C., Salathe, E. P., Kreasuwan, K., Chantara, S. and Siriwitayakorn, K.: Projected  
599 climate change over Southeast Asia using a WRF regional climate model, *Atmos. Sci. Lett.*, 12, 213-  
600 219, 2011.

601

602 Davis, C., Wang, W., Chen, S. S., Chen, Y., Corbosiero, K., DeMaria, M., Dudhia, J., Holland, G.,  
603 Klemp, J., Michalakes, J., Reeves, H., Rotunno, R., Snyder, C. and Xiao, Q.: Prediction of  
604 Landfalling Hurricanes with the Advanced Hurricane WRF Model, *Mon. Wea. Rev.*, 136, 1990-2005,  
605 2008.

606

607 Done, J., Davis, C. A. and Weisman, M.: The next generation of NWP: explicit forecasts of  
608 convection using the weather research and forecasting (WRF) model, *Atmosph. Sci. Lett.*, 5, 100-117,  
609 2004.

610

611 Emanuel, K. A.: A scheme for representing cumulus convection in large-scale models, *J. Atmos. Sci.*  
612 48, 2313-2335, 2001.

613

614 Grell, G. A. and Dévényi, D.: A generalized approach to parameterizing convection combining  
615 ensemble and data assimilation techniques, *Geophys. Res. Lett.*, 29(14), 2002.

616

617 Hong, S.-Y., Noh, Y. and Dudhia, J.: A New Vertical Diffusion Package with an Explicit Treatment of  
618 Entrainment Processes, *Mon. Wea. Rev.*, 134, 2318–2341, 2006

619

620 Hoskins, B. J., Fonseca, R. M., Blackburn, M. and Jung, T.: Relaxing the Tropics to an ‘observed’  
621 state: analysis using a simple baroclinic model, *Quart. J. Roy. Meteor. Soc.*, 138, 1618-1626, 2012.

622

623 Huffman, G. J., Alder, R. F., Bolvin, D. T., Gu, G., Nelkin, E. J., Bowman, K. P., Hong, Y., Stocker,  
624 E. F. and Wolff, D. B.: The TRMM multisatellite image precipitation analysis (TMPA). Quasi-global,

625 multi-year, combined-sensor precipitation estimates at fine scales, *J. Hydrometeor.*, 8, 38-55, 2007.

626

627 Iacono, M. J., Delamere, J. S., Mlawer, E. J., Shephard, M. W., Clough, S. A. and Collins, W. D.:  
628 Radiative forcing by long-lived greenhouse gases: Calculations with the AER radiative transfer  
629 models, *J. Geophys. Res.*, 113, D13103, doi:10.1029/2008JD009944, 2008.

630

631 Janjić, Z. I.: The step-mountain eta coordinate model: further developments of the convection, viscous  
632 sublayer and turbulence closure schemes, *Mon. Wea. Rev.*, 122, 927-945, 1994.

633

634 Kain, J. S.: The Kain-Fritsch convection parameterization: an update, *J. Appl. Meteorol.*, 43, 170-181,  
635 2004.

636

637 Kain, J. S. and Fritsch, J. M.: A one-dimensional entraining/detraining plume model and its  
638 application in convective parameterization, *J. Atmos. Sci.*, 47, 2784-2802, 1990.

639

640 Kain, J. S. and Fritsch, J. M.: Convective parameterization for mesoscale models: the Kain-Fritsch  
641 scheme. *The Representation of Cumulus Convection in Numerical Models*, *Meteorol. Monogr.*, 24,  
642 165-170, Amer. Meteor. Soc., 1993.

643

644 Koh, T.-Y., Wang, S. and Bhatt, B. C.: A diagnostic suite to assess NWP performance, *J. Geophys.*  
645 *Res.*, 117, D13109, doi:10.1029/2011JD017103, 2012.

646

647 Lim, K., Hong, S.: Development of an effective double-moment cloud microphysics scheme with  
648 prognostic cloud condensation nuclei (CCN) for weather and climate models, *Mon. Wea. Rev.*, 138,  
649 1587–1612, 2010.

650

651 Miguez-Macho, G., Stenchikov, G. L. and Robock, A.: Regional climate simulations over North-  
652 America: interaction of local processes with improved large-scale flow, *J. Climate.*, 18, 1227-1246,

653 2005.

654

655 Monin, A. S. and Obukhov, A. M.: Basic laws of turbulent mixing in the ground layer of the  
656 atmosphere, *Trans. Geophys. Inst. Akad. Nauk USSR*, 151, 163-187, 1954.

657

658 Ramage, C. S.: The role of a tropical “maritime continent” in the atmospheric circulation, *Mon. Wea.*  
659 *Rev.*, 96, 365–370, 1968.

660

661 Saha, S., Moorthi, S., Pan, H.-L., Wu, X., Wang, J., Nadiga, S., Tripp, P., Kistler, R., Woollen, J.,  
662 Behringer, D., Liu, H., Stokes, D., Grumbine, R., Gayno, G., Wang, J., Hou, Y.-T., Chuang, H.-Y.,  
663 Juang, H.-M. H., Sela, J., Iredell, M., Treadon, R., Kleist, D., Delst, P. V., Keyser, D., Derber, J., Ek,  
664 M., Meng, J., Wei, H., Yang, R., Lord, S., Dool, H., Kumar, A., Wang, W., Long, C., Chelliah, M.,  
665 Xue, Y., Huang, B., Schemm, J.-K., Ebisuzaki, W., Lin, R., Xie, P., Chen, M., Zhou, S., Huggins, W.,  
666 Zou, C.-Z., Liu, Q., Chen, Y., Han, Y., Cucurull, L., Reynolds, R. W., Rutledge, G. and Goldberg, M.:  
667 The NCEP Climate Forecast System Reanalysis, *Bull. Amer. Meteor. Soc.*, 91, 1015-1057, 2010.

668

669 Samala, B. K., Nagaraju, C., Banerjee, S., Kaginalkar, S.A. and Dalvi, M.: Study of the Indian  
670 summer monsoon using WRF–ROMS regional coupled model simulations, *Atmosph. Sci. Lett.*, 14,  
671 20–27, doi:10.1002/asl2.409, 2013.

672

673 Skamarock, W. C., Klemp, J. B., Dudhia, J., Gill, D. O., Barker, D. M., Duda, M. G., Huang, X.-Y.,  
674 Wang, W. and Powers, J. G.: A description of the Advanced Research WRF version 3, NCAR tech.  
675 Note TN-4175\_STR, 113pp, 2008.

676

677 Stauffer, D. R. and Seaman, N. L.: Use of four-dimensional data assimilation in a limited area  
678 mesoscale model. Part I: experiments with synoptic-scale data, *Mon. Wea. Rev.*, 118, 1250-1277,  
679 1990.

680

681 Stauffer, D. R., Seaman, N. L. and Binkowski, F. S.: Use of four-dimensional data assimilation in a  
682 limited-area mesoscale model. Part II: effects of data assimilation within the planetary boundary layer,  
683 *Mon. Wea. Rev.*, 119, 734-754, 1991.

684

685 Steele, C. J., Dorling, S. R., von Glasow, R. and Bacon, J.: Idealized WRF model sensitivity  
686 simulations of sea breeze types and their effects on offshore windfields, *Atmos. Chem. Phys.*, 13, 443-  
687 461, DOI: 10.5194/acp-13-443-2013, 2013.

688

689 Teo, C.-K., Koh, T.-Y., Lo, J. C.-F. and Bhatt, B. C.: Principal Component Analysis of observed and  
690 modelled diurnal rainfall in the Maritime Continent, *J. Climate*, 24, 4662-4675, 2011.

691

692 Tetens, V.O.: Uber einige meteorologische. Begriffe, *Zeitschrift fur Geophysik*, 6, 297-309, 1930.

693

694 Waldron, K. M., Peagle, J. and Horel, J. D.: Sensitivity of a spectrally filtered and nudged limited area  
695 model to outer model options, *Mon. Wea. Rev.*, 124, 529-547, 1996.

696

697 Ummenhofer, C. C., England, M. H., McIntosh, P. C., Meyers, G. A., Pook, M. J., Risbey, J. S.,  
698 Gupta, A. S. and Taschetto, A. S.: What causes Southeast Australia's worst droughts?, *Geophys. Res.*  
699 *Let.*, 36(4), L04706, doi:10.1029/2008GL036801, 2009.

700

701 von Storch, H., Langenberg, H. and Feser, F.: A spectral nudging technique for dynamical  
702 downscaling purposes, *Mon. Wea. Rev.*, 128, 3664-3673, 2000.

703

704 Zeng, X. and Beljaars, A.: A prognostic scheme of sea surface skin temperature for modeling and data  
705 assimilation, *Geophys. Res. Let.*, 32, L14605, doi:10.1029/2005GL023030, 2005.

706  
707  
708  
709  
710  
711  
712  
713  
714  
715  
716  
717  
718  
719  
720  
721  
722

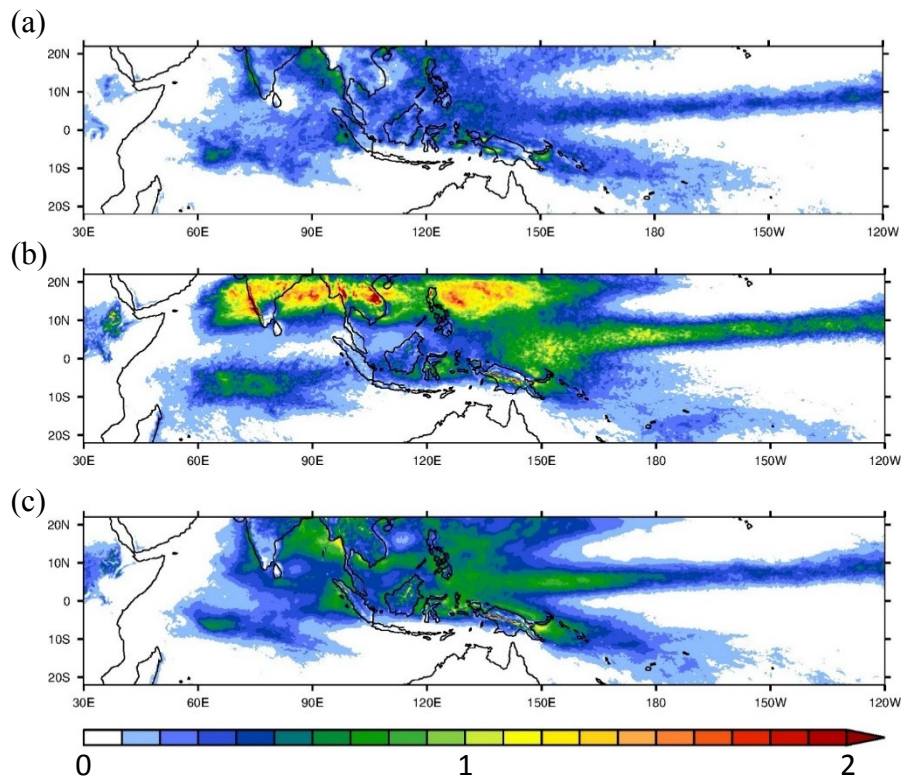


**Figure 1:** Precipitation rate (units of mm hr<sup>-1</sup>) averaged over June to September (JJAS) 2008 from (a) TRMM 3B42 version 6, (b) WRF run with no interior nudging and (c) WRF run with analysis nudging (see text for more details). In all plots the colour bar is linear with only the middle and end values shown.

723

724

725

726

727

728

729

730

731

732

733

734

735

736

737

738

739

740

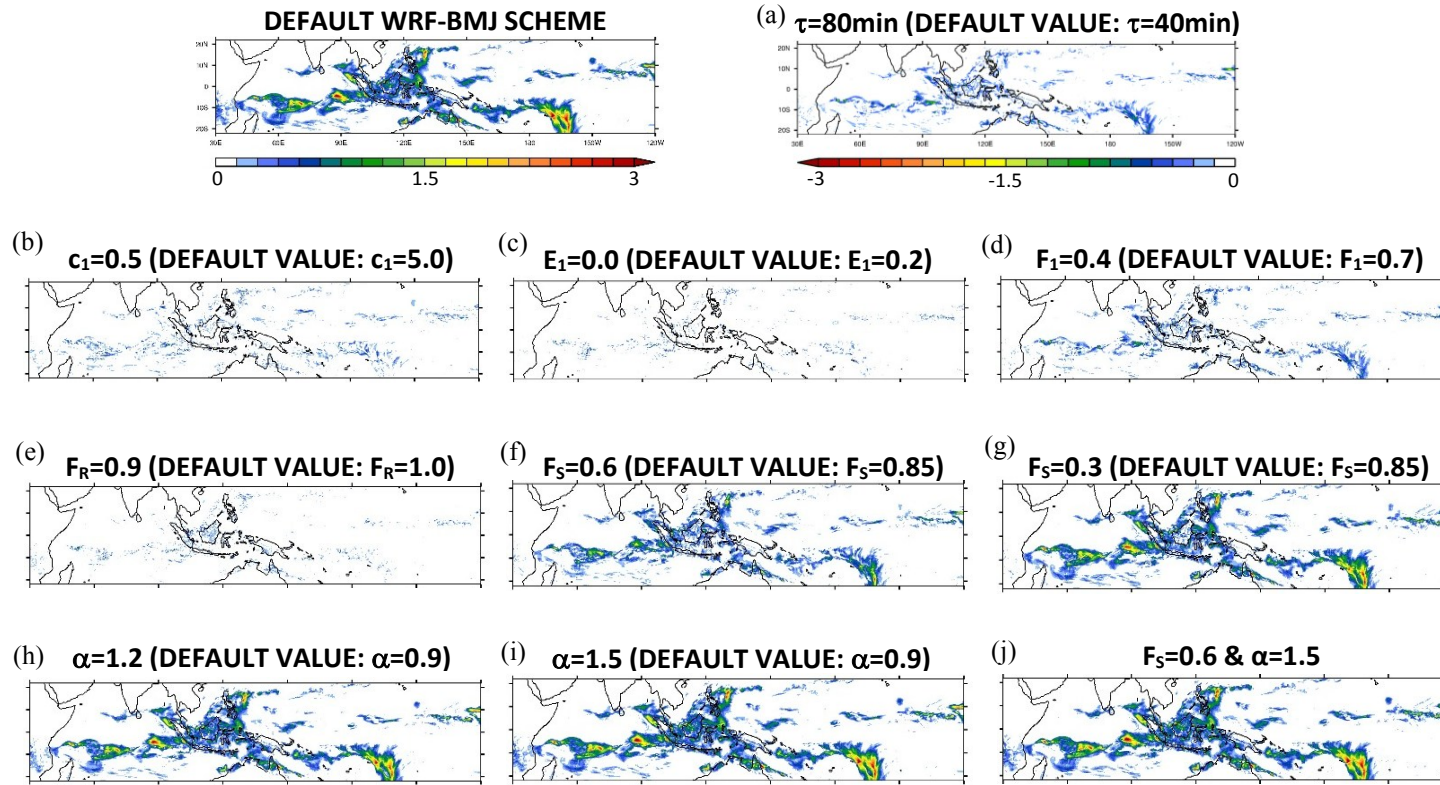
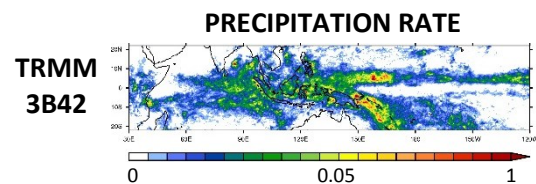


**Figure 2:** Precipitation rate from a 1-day WRF run (from 00UTC on 2<sup>nd</sup> March to 00UTC on 3<sup>rd</sup> March 2008) with the default WRF-BMJ and modification in the rainfall rate for ten experiments with a modified BMJ scheme using separately (a)  $\tau=80\text{min}$ , (b)  $c_1=0.5$ , (c)  $E_1=0.0$ , (d)  $F_1=0.4$ , (e)  $F_R=0.9$ , (f)  $F_S=0.6$ , (g)  $F_S=0.3$ , (h)  $\alpha=1.2$ , (i)  $\alpha=1.5$  and (j)  $F_S=0.6$  and  $\alpha=1.5$  (units of  $\text{mm hr}^{-1}$ ). The conventions are as in *Figure 1*. Note that the colour scale is reversed to show drying upon modifications.

741

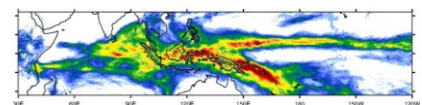
742

743



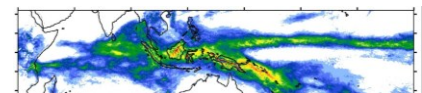
744

**DEFAULT**  
**WRF-BMJ**



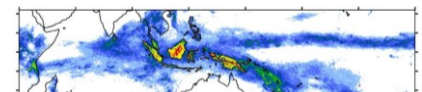
745

**MODIFIED**  
**BMJ ( $F_s=0.6$ )**



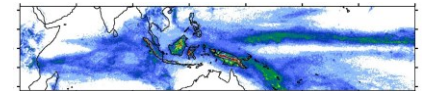
746

**MODIFIED**  
**BMJ ( $F_s=0.3$ )**



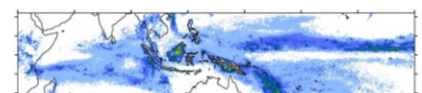
748

**MODIFIED**  
**BMJ ( $\alpha=1.2$ )**



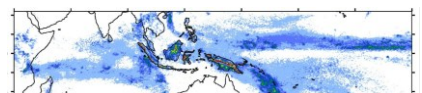
749

**MODIFIED**  
**BMJ ( $\alpha=1.5$ )**



750

**MODIFIED BMJ**  
**( $F_s=0.6$  &  $\alpha=1.5$ )**



752

753

754

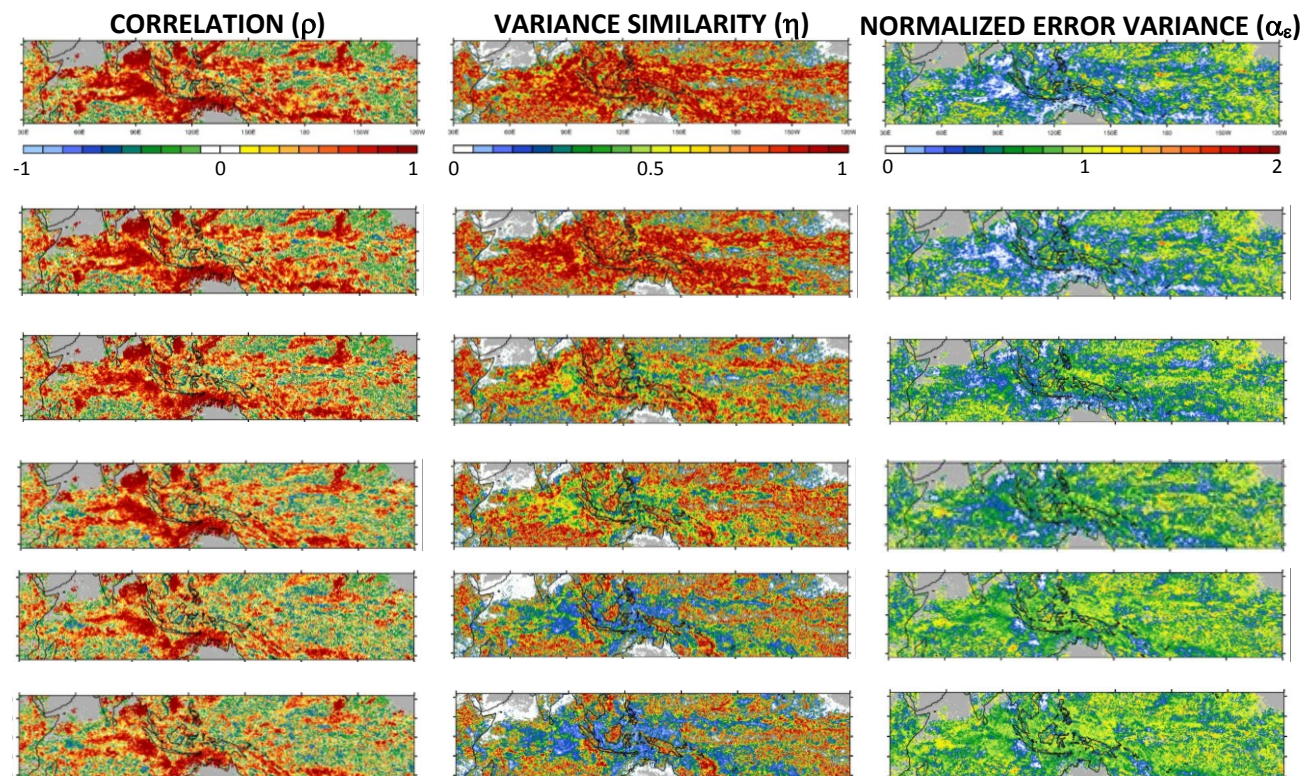
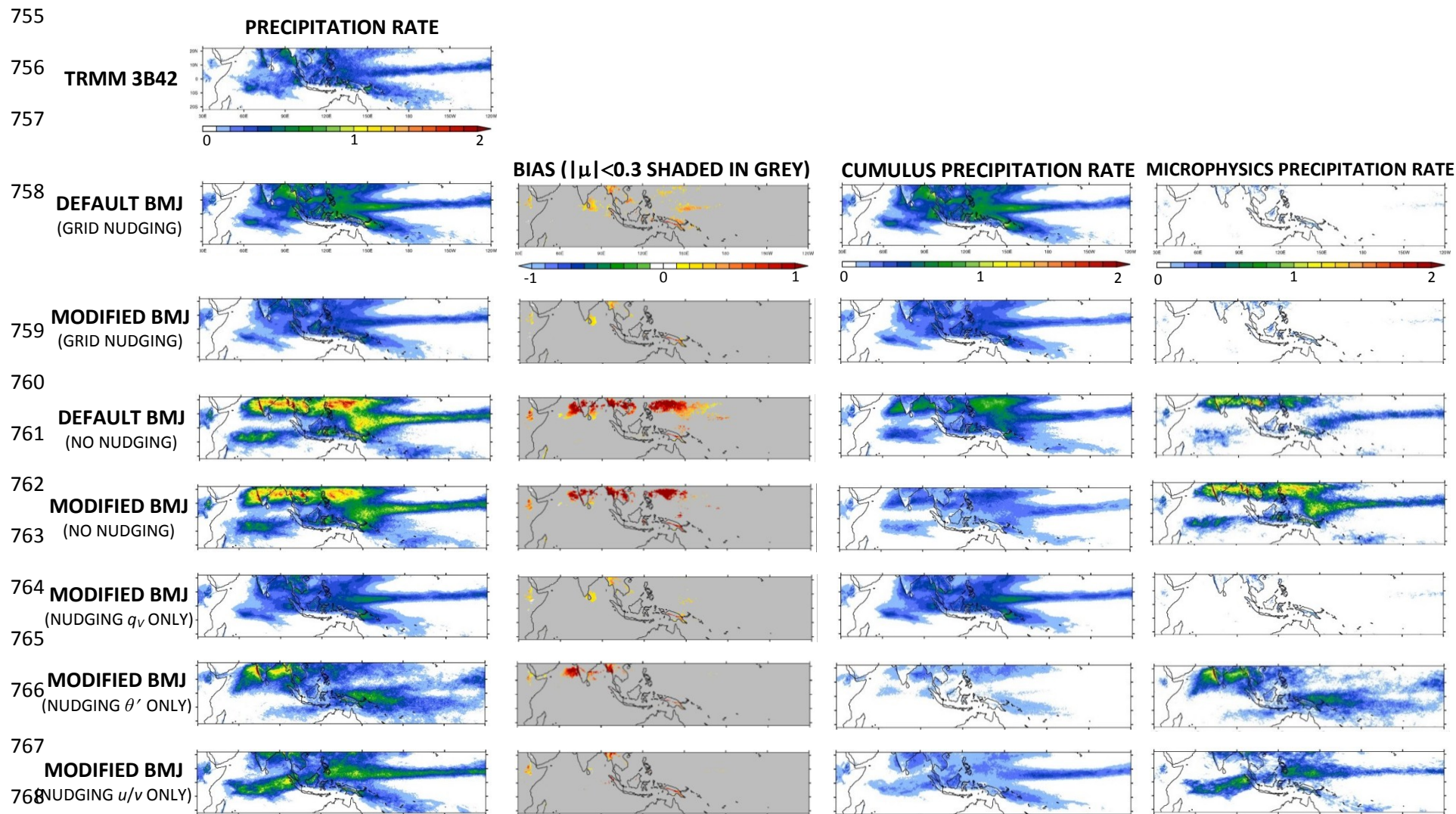


**Figure 3:** Precipitation rate ( $\text{mm hr}^{-1}$ ) from TRMM and WRF and model correlation ( $\rho$ ), variance similarity ( $\eta$ ) and normalized error variance ( $\alpha_\epsilon$ ) with respect to TRMM for the experiments with the default BMJ scheme and with five modified versions of the BMJ scheme averaged over April 2008. The conventions are as in *Figure 1* with regions where  $\rho$ ,  $\eta$  and  $\alpha_\epsilon$  are infinite shaded in grey.



769 **Figure 4:** Precipitation rate ( $\text{mmhr}^{-1}$ ) averaged over JJAS 2008 from TRMM and 7 WRF experiments with the default BMJ and modified BMJ ( $F_S=0.6$ ) schemes both with and without analysis nudging and relaxing only the water vapour mixing ratio ( $q_v$ ), horizontal winds ( $u,v$ ) and potential temperature perturbation ( $\theta'$ ) in the interior of the domain separately towards CFSR. *Left to right:* precipitation rate, model bias (regions where  $|\mu| < 0.3$  are shaded in grey) with respect to TRMM and precipitation rate from the cumulus and microphysics schemes. The conventions are as in *Figure 1*.

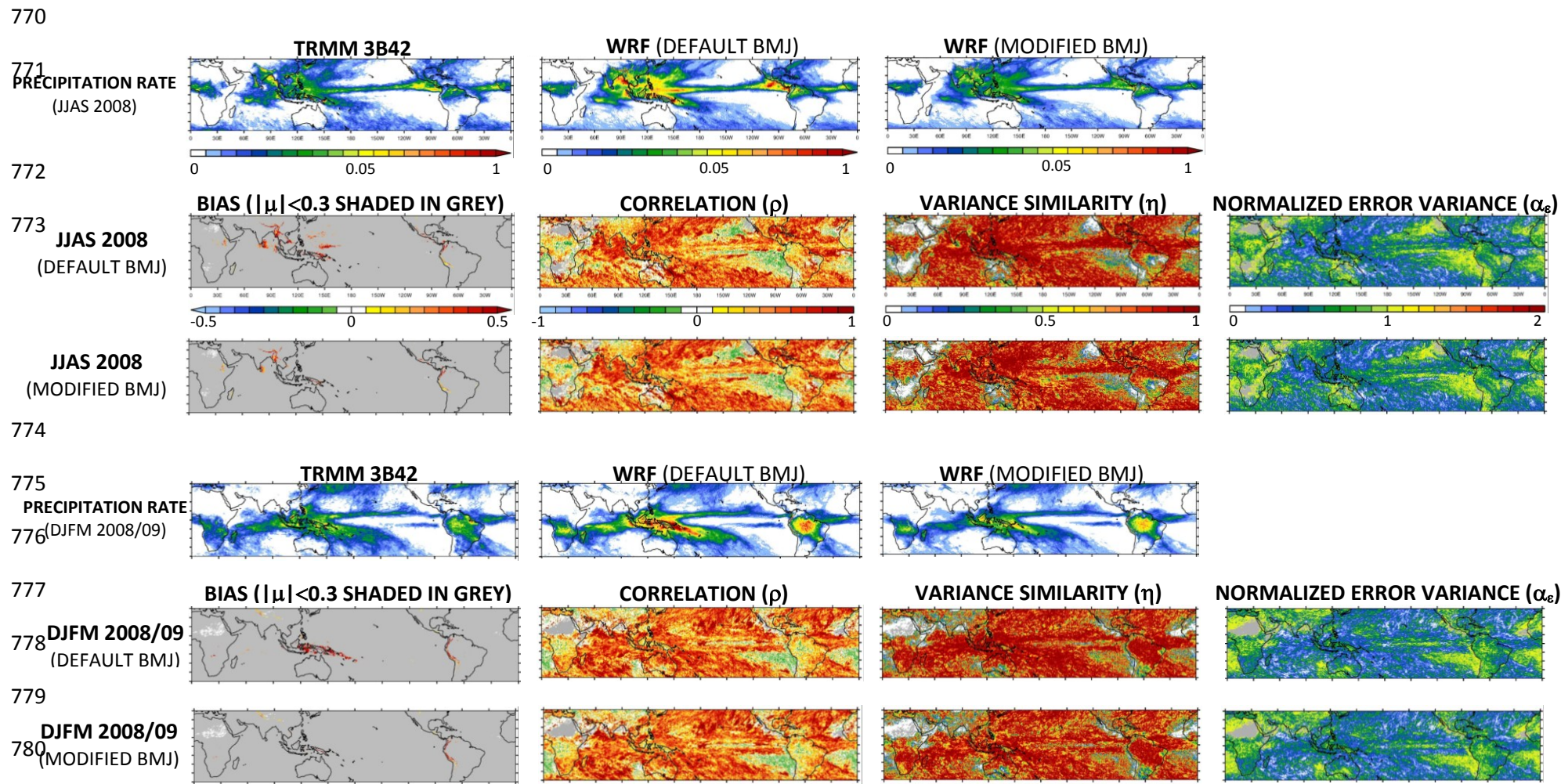


**Figure 5:** Precipitation rate ( $\text{mmhr}^{-1}$ ) from TRMM and WRF and model biases (regions where  $|\mu| < 0.3$  are shaded in grey), correlation ( $\rho$ ), variance similarity ( $\eta$ ) and normalized error variance ( $\alpha_\epsilon$ ) with respect to TRMM for the tropical belt experiments with analysis nudging and the default and modified BMJ schemes averaged over JJAS 2008 and DJFM 2008/2009. The conventions are as in *Figure 1* and, as in *Figure 3*, regions where  $\rho$ ,  $\eta$  and  $\alpha_\epsilon$  are infinite are shaded in grey.